Netherlands Institute of Applied Geoscience TNO
- National Geological Survey

Princetonlaan 6
P.O. Box 80015
3508 TA Utrecht

www.tno.nl

P +31 30 2564600
F +31 30 2564605
info@nitg.tno.nl

TNO report

NITG 03-064-B

Interpretation of the 1999 and 2001 time-lapse seismic data (WP 5.4)

Date	20 February 2003
Author(s)	Rob Arts (TNO) Andy Chadwick (BGS) Ola Eiken (Statoil) Peter Zweigel (Sintef)
Copy no	
No. of copies	
Number of pages	32
Number of appendices	
Sponsor	European Commission
Project name	SACS
Project number	005.72029

Contents

1 Introduction

Since October 1996, Statoil and its Sleipner partners have injected CO_2 into a saline aquifer, the Utsira Sand, at a depth of 1012 m below sea level. The CO_2 is separated on the platform from natural gas produced at the Sleipner field in the central North Sea (Norwegian block 15/9) and injected into the aquifer through a highly deviated well at a lateral distance of about 2.3 km from the platform (Figure 1).

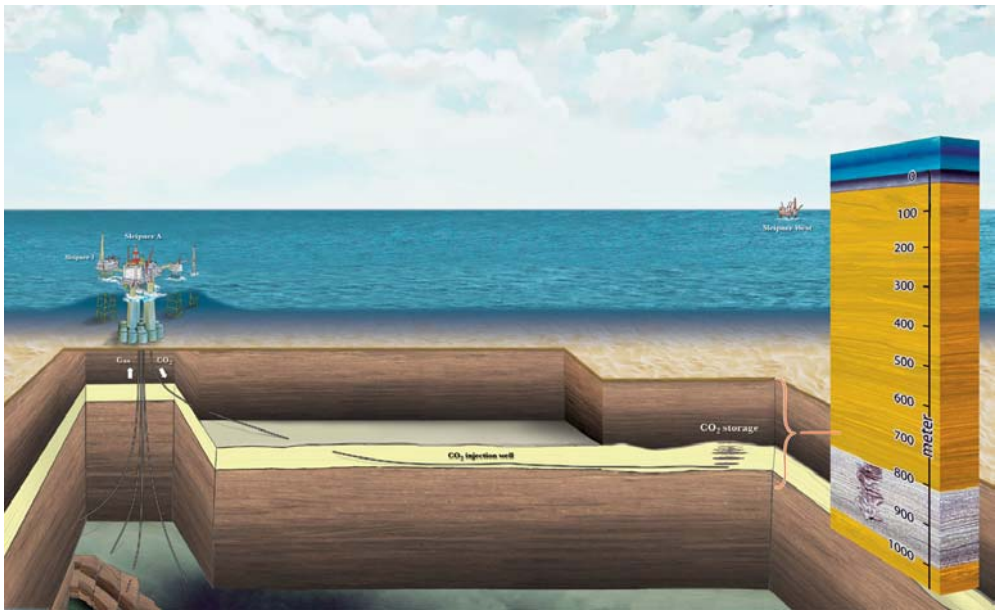

Figure 1: CO_2 injection scheme.

A multi-institutional research project SACS (Saline Aquifer CO_2 Storage) was formed to predict and monitor the migration of the injected CO_2. Two time-lapse seismic surveys over the injection area have been acquired, one in October 1999 after 2.35 million tonnes of CO_2 had been injected and the second in October 2001 after 4.26 million tonnes of CO_2 had been injected. Comparison with the baseline seismic survey of 1994 prior to injection provides detailed insights into the subsurface distribution and migration of the CO_2.

Within the SACS 1&2 projects and the SACS 2 TFE addendum TNO, BGS, Statoil and Sintef have carried out the interpretation of the time-lapse seismic data obtained over the injection site (Task 5.4). The work of TNO, BGS and Statoil has been concentrated on the post-stack data, whereas Sintef has mainly worked with the pre-stack data (Tasks 5.5 & 5.7). The latter is reported separately.

Chapter 2 gives a short overview of the geological background information relevant to the interpretation of the time lapse seismic data. Chapter 3 describes modelling results necessary to explain the seismic observations such as interference and pushdown. Chapter 4 gives an overview of the actual interpretation of the time lapse seismic data in terms of CO_2 distribution. A more quantitative approach to the interpretation is given in Chapter 5. Finally the link of the interpretation to results of the reservoir simulation is given in Chapter 6 followed by a general discussion on the results in Chapter 7.

2 Background information

2.1 Geology of the Utsira Sand in the Sleipner area

The Utsira Sand forms part of the Mio-Pliocene Utsira formation (Gregersen et al. 1997, Chadwick et al. 2001), and is overlain by a thick, dominantly shaly, overburden. Four key reflectors based on well information have been interpreted on the 1994 baseline survey (Arts et al. 2000, 2001), top Pliocene prograding unit, intra-Pliocene prograding unit, top Utsira Sand and base Utsira Sand (Figure 2).

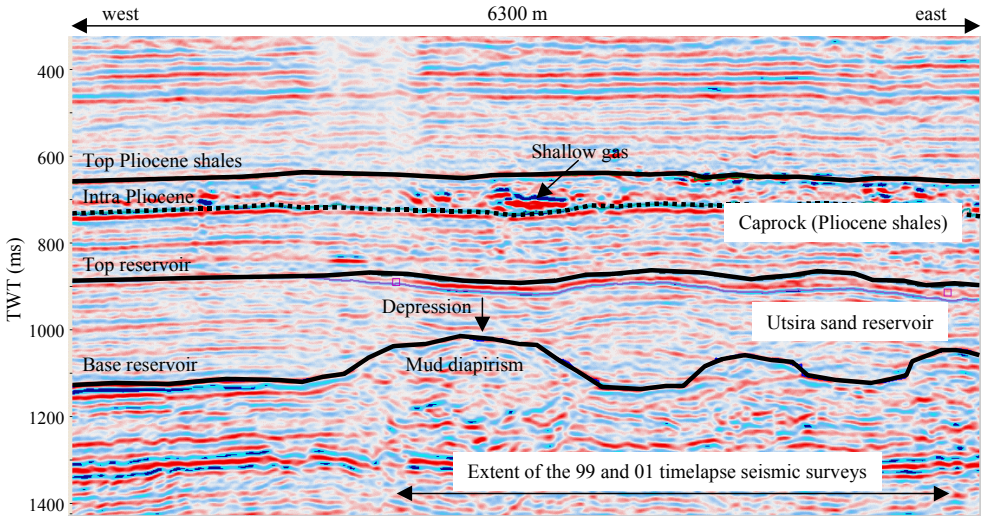

Figure 2: Key horizons interpreted on the 1994 baseline survey. The arrow at the bottom indicates the extent of the 1999 and the 2001 time lapse seismic surveys.

The Utsira Sand has a thickness of more than 200 m near the injection site but laterally shows marked thickness variation. Mounds at its base are interpreted as due to mud diapirism active during deposition of the lower part of the Utsira Sand. The presence of these shale mounds induced differential compaction, which led to depressions forming in the Utsira Sand and overlying units above the mud volcanoes (Figure 2). These depressions constitute local modifications of the general southward dip of the top Utsira Sand, and include local domal and anticlinal structures, which act as potential traps and/or channels for CO_2 flow.

Within the Utsira Sand, several thin shale layers with an average thickness of 1 to 1.5 m have been identified from well log data. Although they are not resolved on the baseline (pre-injection) seismic data, it is possible to establish a wireline correlation between the "shale peaks" in closely spaced wells over distances up to 1 km (Zweigel et al. (in press), Arts et al. 2000, 2001). About 20 m below the top of the reservoir a thicker shale unit of 5 to 7 m thick (hereafter referred to as the 'five metre shale') is present. In previous publications the sand unit above this thicker shale layer has been referred to informally as the "sandwedge". However because the upper sand is more correctly considered as part of the main Utsira reservoir, the term "sandwedge" will no longer be used.

The Pliocene shales of the caprock can be subdivided into two units separated by the intra-Pliocene horizon. The lower unit, directly overlying the Utsira Sand, includes at its base a shale drape, termed the Lower Seal, that can be distinguished on a regional scale. This lower unit exhibits locally anomalously high amplitudes. The upper Pliocene prograding unit is characterized by irregular internal reflectors and some very high amplitudes which might be due to the presence of shallow gas.

2.2 The injection operation

CO_2 is injected near the base of the Utsira Sand at depths of 1010-1013 m below sea level, within a 38 m long well perforation interval. The main mechanism driving flow of the CO_2 is gravity, the CO_2 rising buoyantly until it reaches an intra-reservoir shale (Lindeberg et al. 2001). These thin shale layers form at least temporary flow-barriers for the CO_2, but are not expected to be fully tight (Zweigel et al. (in press)). Reservoir simulations (van der Meer et al. 2001) indicate that most of the CO_2 remains trapped in relatively thin, high saturation accumulations beneath the shale layers and follows their topography. An example of a reservoir simulation at the time of the 1999 time-lapse seismic survey is shown in Figure 3 as an illustration.

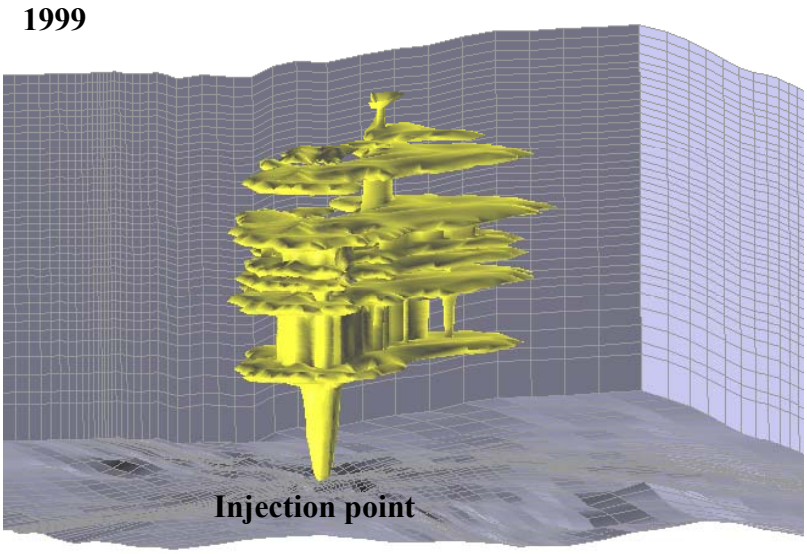

Figure 3: Result of a reservoir simulation at the time of the first time lapse seismic survey in October 1999 (after 3 years of injection) after 2.28 million tonnes of CO_2 injected.

3 Modelling of the seismic response

3.1 Petrophysical properties of the Utsira Sand reservoir

The petrophysical properties of the Utsira Sand pertinent to its seismic response have been determined from well log data (Figure 4). The Utsira Sand is a very weakly cemented sandstone with measured porosities in the range 30 to 42% (mean value 37%). The acoustic velocity in the water-saturated sandstone is on average 2050 ms^{-1} with variations and uncertainty in the range 1950 to 2100 ms^{-1}. Bulk densities of water-saturated Utsira Sand have been estimated in the range 1960 to 2080 kgm^{-3}.

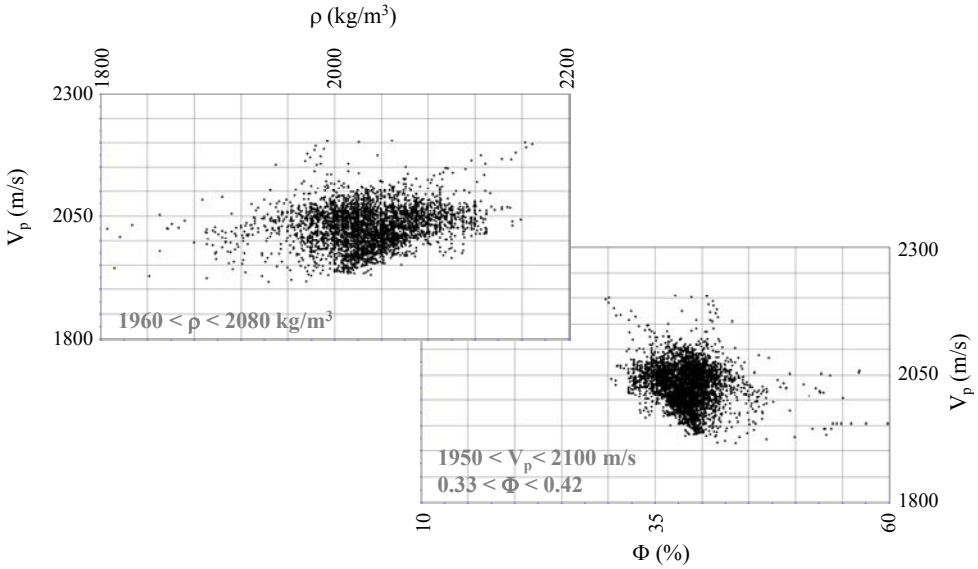

Figure 4: Crossplots of the compressional wave velocity (Vp) versus the bulk density (ρ) and the porosity (ϕ) of the Utsira Sand derived from 14 wells in the Sleipner area.

Norwegian well 15/9-A23 is the only well in the Sleipner area with shear wave velocity information through a DSI-log. The average value of the shear wave velocity is 643 ms^{-1}, varying in the range 600 to 680 ms^{-1} (Figure 5).

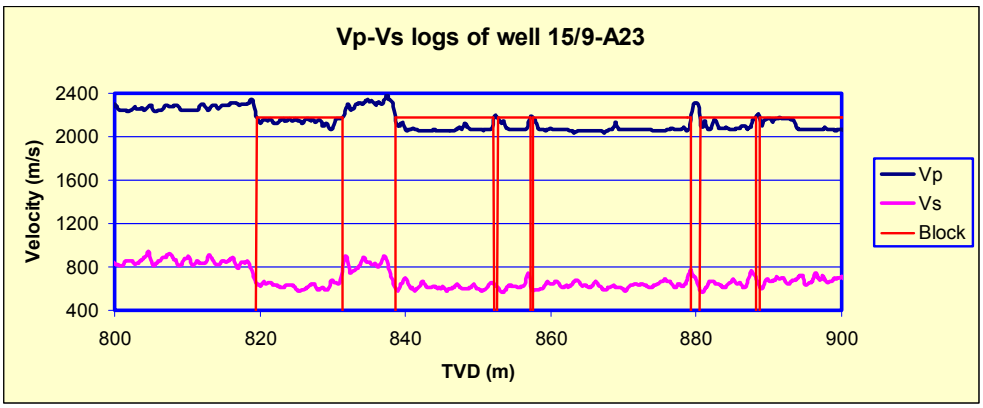

Figure 5: Vp-Vs logs of well 15/9-A23. The red blocks indicate the Utsira Sand intervals. The remainder forms the shales.

3.2 Petrophysical properties of the caprock and of the intra-reservoir shale layers

For seismic modelling purposes, estimates of the P- and S-wave velocities and of the bulk density of the caprock and of the intra-reservoir shale layers are required. Values for the caprock have been estimated from well log data which indicate a P-wave velocity of Vp = 2270ms^{-1}, an S-wave velocity of Vs = 850 ms^{-1} (Figure 5) and a bulk density of ρ = 2100 kgm^{-3}. Uncertainties and variations are estimated in the order of 4%. The well log expression (including the sonic and density) of the intra-reservoir shale "spikes" is similar to the log-response of the Pliocene caprock shales, so the same values have been used (Zweigel et al., in press).

3.3 Petrophysical properties of the injected CO_2

The natural pressure and temperature at the injection point are estimated at 10 MPa and 36 degrees Celsius respectively. Under these conditions CO_2 is in a supercritical state. In practice this means that it has the density of a fluid, but the compressibility of a gas. The most likely values for the density of the CO_2 are between 600 and 700 kgm^{-3}. The bulk modulus of the CO_2 can vary in a certain range as well under the given circumstances. Especially the upper limit is important for the geophysical purpose and is considered likely to have a value not greater than 0.07 GPa.

3.4 Gassmann modelling

Seismic velocities were modelled as a function of CO_2 saturation from the Gassmann relationships (Gassmann, 1951) which enable the elastic properties of a porous medium saturated with a fluid to be derived from the known properties of the same medium saturated with a different fluid. As a basic assumption in this analysis homogeneous mixtures of brine and CO_2 with respect to the seismic wavelength are assumed. In reality this condition is likely to be only approximately fulfilled. The densities and compressibilities of the saturating fluids, the rock matrix and the porosity of the rock are assumed to be known.
In the Sleipner case the 100% water-saturated P- and S-wave velocities are known from well logs. The main constituent of the rock matrix is quartz with a known density and compressibility. The sand porosity, and the densities and compressibilities of the water and of the CO_2 are also known. From this information, the Gassman relationships can be used to calculate the elastic velocities (P- and S-wave) and the density of the rock, saturated with a CO_2 -water mixture, for a range of saturation states.

Because of the uncertainty in the bulk modulus of the CO_2 under reservoir conditions, velocities have been calculated for three values within extreme limits (Figure 6). For values of $Kco_2 \leq 0.07$ GPa velocities are fairly constant for CO_2 -saturations over 20%. For higher bulk moduli, the elastic properties of CO_2 more closely resemble those of the replaced water and the effect on seismic velocity decreases.

In general it is clear, that even for small CO_2 saturations, the drop in P-wave velocity is considerable (about 30%). This can be explained by the fact that relatively few small "bubbles" of CO_2 have a dramatic effect on the overall compressibility of the saturated rock. Therefore a sharp decrease in the P-wave velocity can be observed for small CO_2 concentrations.

The influence of the CO_2 on the S-wave velocities is minimal because shear waves are not sensitive to the saturating fluids. The minor variation that is observed is due to the variation in the bulk density (CO_2 is less dense than water).

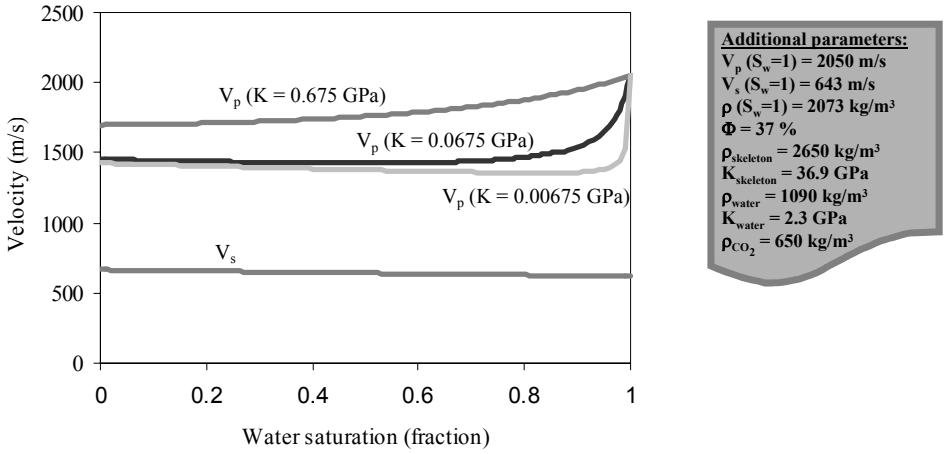

Figure 6: Elastic velocities of the Utsira Sand as a function of water- CO_2 -saturation using Gassmann's model. The required input parameters are reported including three extreme values for the bulk modulus of the CO_2.

3.5 Pressure effect

During the injection process at Sleipner, until 2001 no significant increase in well head pressure has been observed at the injection well (not exceeding the unsystematic data scatter of about 0.2 MPa), the CO_2 flowing easily into the very high permeability reservoir. The pressure-temperature conditions of the reservoir around the CO_2 plume are such that the CO_2 is expected to remain in a dense (liquid or supercritical) phase. Based on downhole measurements the estimated formation temperatures increase from 29 C at the top of the reservoir to 36 C at the base of the reservoir. Taking this into consideration, the pressure effect on the seismic velocities is expected to be marginal.

3.6 Wavelet determination and synthetic modelling

The frequency content of the baseline seismic shows a bandwidth from approximately 10 to 70 Hz with a central peak frequency of around 40 Hz (Arts, 2000).
In order to perform seismic modelling, a wavelet was estimated from the seismic data. Assuming zero phase data, the wavelet was computed from the spectra at various inlines in order to check the spatial variability of the estimated wavelet. The results show no significant variation, leading to an optimum mean wavelet.

Using the estimated elastic parameters for the shale layers, for the 100% water-saturated sandstone and for the 100% CO_2 -saturated sandstone, a simplified acoustic impedance model was created in order to illustrate the seismic response of the injected CO_2. Figure 7 shows an example of CO_2 accumulating at the top of the reservoir and beneath two illustrative intra-reservoir shale layers. A range of CO_2 thicknesses was modelled in order to investigate the influence on the seismic signal (Arts et al., 2002, (in press)).

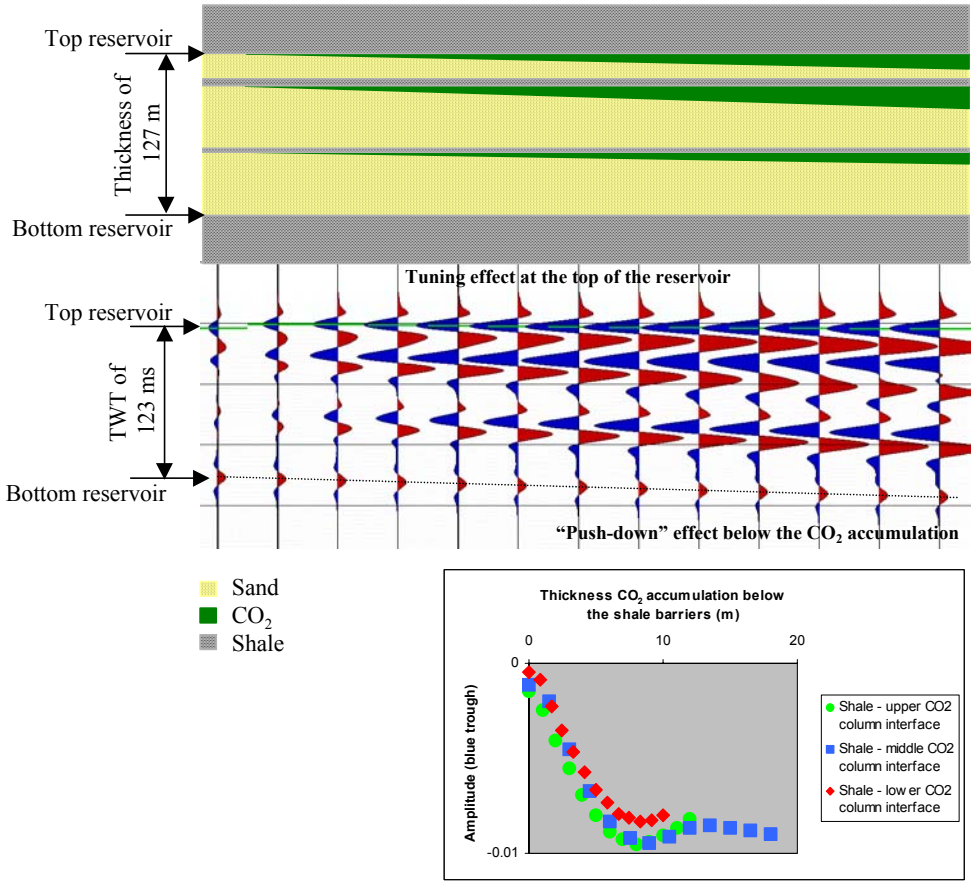

Figure 7: Illustrative model of injected CO_2 trapped in a simplified reservoir scenario representative of the Sleipner case. The thickness of the CO_2 layers increases rightwards and the corresponding synthetic seismic response is shown below. At the bottom the amplitudes of the synthetic seismic signals caused by the three CO_2 accumulations are plotted as a function of the CO_2 layer thickness. The so-called tuning thickness corresponds to a CO_2 column of 8 m. Note the increase in seismic energy above the actual top of the reservoir caused by tuning in the thickening layer of CO_2.

Two dominant effects determine the seismic response:

- The negative seismic impedance contrast between shale and underlying sand becomes more negative (larger in absolute value) when CO_2 is present in the sand.
- The seismic response is a composite wavelet caused by interference from sequences of water-saturated sand, shale, CO_2 -saturated sand and water-saturated sand again.

The first effect leads to stronger negative seismic amplitudes as for a classical "bright spot". The second effect (tuning) can lead to destructive or constructive interference depending on the thickness of the CO_2 layer, evident from the seismic modelling (Figure 7). As the thickness of the CO_2 column increases from 0 to 8 m a gradual increase of the (negative) amplitude is observed. Maximum constructive interference corresponds to a CO_2 thickness of about 8 m, the so-called 'tuning thickness'

3.7 Tuning effect at the top of the reservoir

At the top of the reservoir an interesting phenomenon is observed. Due to the tuning effect of CO_2 trapped at the top of the Utsira Sand, the main reflection trough appears to be aligned slightly above the reservoir top for thin CO_2 accumulations. Modelling shows (Figure 7) that the tuning effect can displace the peak upward by as much as 3 ms two-way time (Arts et al. (in press)).

3.8 Velocity "push-down" effect

Below the CO_2 plume a prominent velocity "push down" is expected due to the lower velocities through the CO_2 -saturated sand with respect to the water-saturated sand (Eiken et al., 2000, Brevik et al., 2000, Arts et al. 2001, 2002). This effect can be quantified by a so-called "gross pushdown factor". The "gross pushdown factor" has units of sm^{-1} and expresses the amount of pushdown in seconds (or milliseconds) per metre thickness of fully CO_2 -saturated rock. The mathematical expression of the "gross pushdown factor" is:

$$\frac{2\left(V_{S_w} - V_{S_{CO_2}}\right)}{\left(V_{S_w} V_{S_{CO_2}}\right)}$$

To illustrate, using the calculated Gassman velocities, if a 10 m column of fully water-saturated sand were replaced by a 10 m column of fully CO_2 -saturated sand, the resulting TWT pushdown or time-delay, would be about 4 ms.

4 Time-lapse seismic observations

4.1 Observed seismic reflectivity

Introducing CO_2 into the Utsira reservoir has a dramatic effect on reflectivity. The 1994 pre-injection data (Figure 8), show moderate reflections from the top and base of the reservoir, with much weaker intra-reservoir events (the mid-Utsira reflection is a seabed multiple of the prominent events near to the top of the reservoir). The slight domal closure above the injection point is well imaged. In contrast, the 1999 and 2001 data show a clear image of the CO_2 plume with strong reflections at a number of levels within the reservoir. These are interpreted as layers of CO_2 accumulating or 'ponding' beneath the thin intra-reservoir shales. The CO_2 related reflections do not show the gentle antiformal geometry of the Utsira stratigraphy as imaged on the 1994 data, but rather show a downward pointing V-profile, which becomes more pronounced down through the reservoir. This is interpreted as an effect of velocity pushdown within the plume. Figure 8 shows an inline through the injection area for the 1994, 1999 and the 2001 surveys including the difference between the 1999-1994 data and the 2001-1994 data.

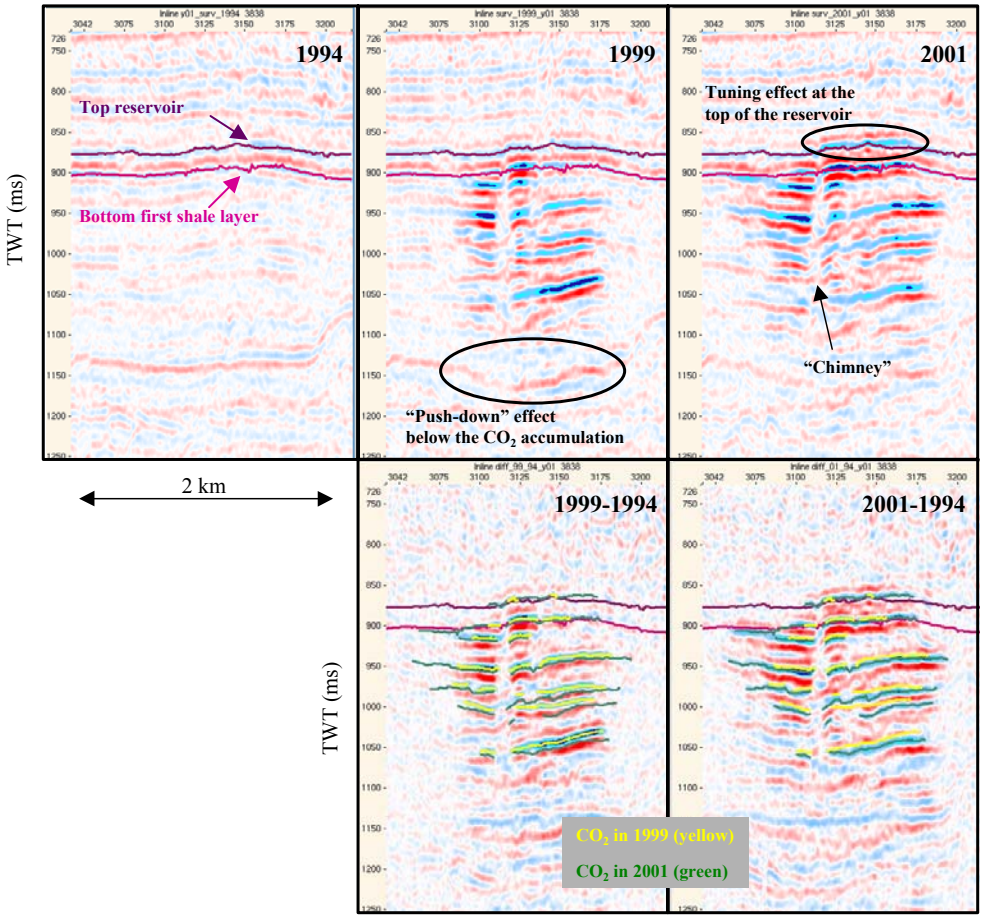

Figure 8: Inline 3838 through the injection area for the 1994, 1999 and the 2001 surveys including the difference between the 1999-1994 data and the 2001-1994 data. The CO_2 levels interpreted in 1999 (yellow) and in 2001 (green) are visualised on both difference sections.

The interpreted CO_2 levels are shown in yellow as interpreted on the 1999 data and in green as interpreted on the 2001 data. The consistency between the 1999 and the 2001 CO_2 levels is obvious. In general the 2001 CO_2 levels have a larger lateral extent and have been "pushed down" slightly more with respect to the 1999 CO_2 levels. The latter can be easily understood considering that more injected CO_2 causes more pushdown.

The difference data also show complex structure within the plume, including vertical linear zones of amplitude reduction and relatively isolated volumes of CO_2 (Figure 8). Reflections on the difference data beneath the injection point are interpreted as artefacts. These have two main causes: multiple energy (principally the seabed multiple) from the overlying plume, and 'difference' signal generated by the effects of velocity pushdown rather than by changes in reflectivity.

The multiples can be recognised by their polarity reversal with respect to CO_2 reflections, but at some locations they interfere with the primary reflections making interpretation very difficult. To derive proper difference sections the seismic datasets would have to be time-depth converted very precisely. So far this has not proved feasible in such detail due to the complicated interference patterns occurring within the "bubble" and the highly accurate velocity model required.

As predicted from seismic modelling, introducing CO_2 into the Utsira Sand has a dramatic effect on the reflectivity. Strong negative reflections are observed at nine stratigrapgical levels both on the 1999- and the 2001 time-lapse surveys. These levels have been numbered from 1 at the deepest level to 9 at the top of the reservoir. Figure 9 shows amplitude maps of the 9 interpreted levels both for the 1999 and the 2001 data.

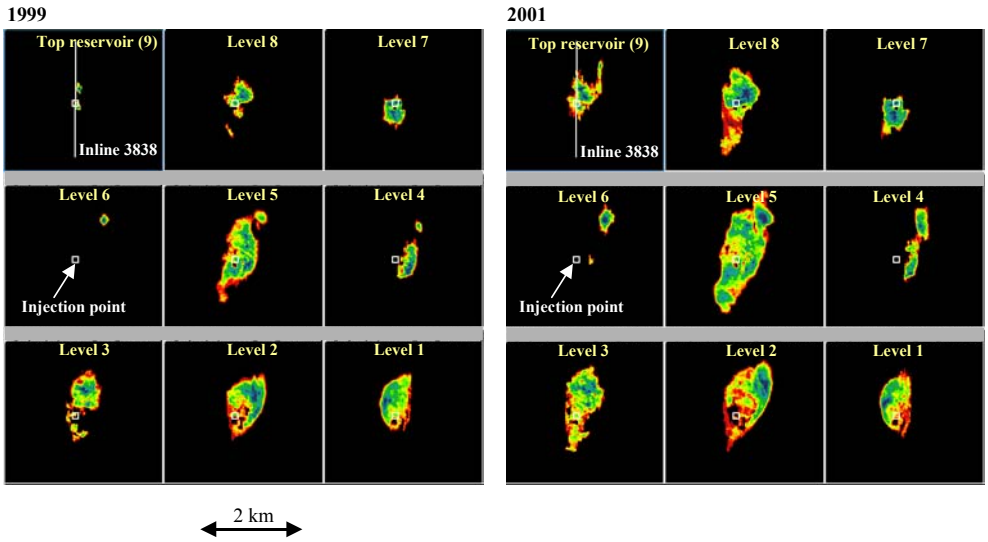

Figure 9: Amplitude maps of the individual CO_2 accumulations in the 1999 seismic data (left image) and in the 2001 data (right image). The levels go down from the shallowest accumulation at the top of the reservoir at level 9 to the deepest at level 1. Location of inline 3838 (Figure 8) also shown.

The observed two highest CO_2 reflections correspond respectively to trapping at the top of the Utsira Sand reservoir (level 9) and trapping beneath the 5 m thick shale layer (level 8). In 1999 the CO_2 had just reached the top of the reservoir. By 2001 the CO_2 had migrated laterally beneath the caprock and the CO_2 reflection appears slightly earlier than the top Utsira Sand reflection (Figure 8). This is likely to be in part due to

the tuning effect described in section 3.7 and possibly also partly due to unresolved stratigraphical complexity at the reservoir top. No evidence has been found of CO_2 migrating significantly into the caprock.
The seven deeper interpreted reflections are caused by CO_2 accumulated beneath the thin intra-reservoir shale layers. Any reflections from these thin shales on the 1994 baseline data are too weak to identify. Only the presence of trapped CO_2 illuminates them sufficiently to make interpretation possible.

4.2 Thin bed effects

The nine picked horizons have a total plan area of about 2.9×10^6 m^2 on the 1999 dataset (Chadwick et al. (in press)). Taking an injected CO_2 volume of 3.3×10^6 m^3, and a mean reservoir porosity of 0.37, if the CO_2 were wholly distributed as reflective sub-horizontal layers, these layers would, on average, be only about 3 m thick. Because CO_2 is also interpreted to be present as chimneys between the layers (see below), the actual average layer thickness would be less than 3 m. With layer thicknesses generally beneath the limit of seismic resolution ($\lambda/4$, ~8 m for these data), the observed CO_2 reflectivity is therefore likely to be largely a consequence of thin-layer interference. With thin-layers, reflection amplitude is related directly to layer thickness, increasing from zero at zero layer thickness, to a maximum at the tuning thickness (Figure 7). This is consistent with observed amplitudes on the picked horizons, which tend to increase systematically inwards, from zero at their outer edges to a maximum value near their centres (e.g. Figure 9). The highest amplitudes moreover, are encountered in the central parts of the most really extensive horizons. These observations all indicate a tuned response from thin layers of CO_2 which thicken from zero at their outer edge to a maximum in the axial part of the plume, within the structural closure. Dominantly thin-layer reflectivity is also consistent with the observed seismic waveforms which comprise mostly interference doublets, rather than the near-symmetrical, near-zero phase processed input wavelet (this is well displayed at simple acoustic interfaces such as the seabed).

The tuning effect is illustrated in Figure 10. For this figure locations have been selected in the 1999 and 2001 survey, where only a single shale layer with CO_2 captured underneath is present. As expected these locations are concentrated towards the outer limits of the whole CO_2 plume. Note that the only criterion is the presence of a single CO_2 accumulation, but not necessarily the same layer everywhere. For these selected locations the “pushdown” in time (which for a single layer is linearly related to the thickness of the CO_2 accumulation) has been plotted against the seismic reflection amplitude. The data appear to follow a tuning relationship as expected from the synthetic seismic modelling.

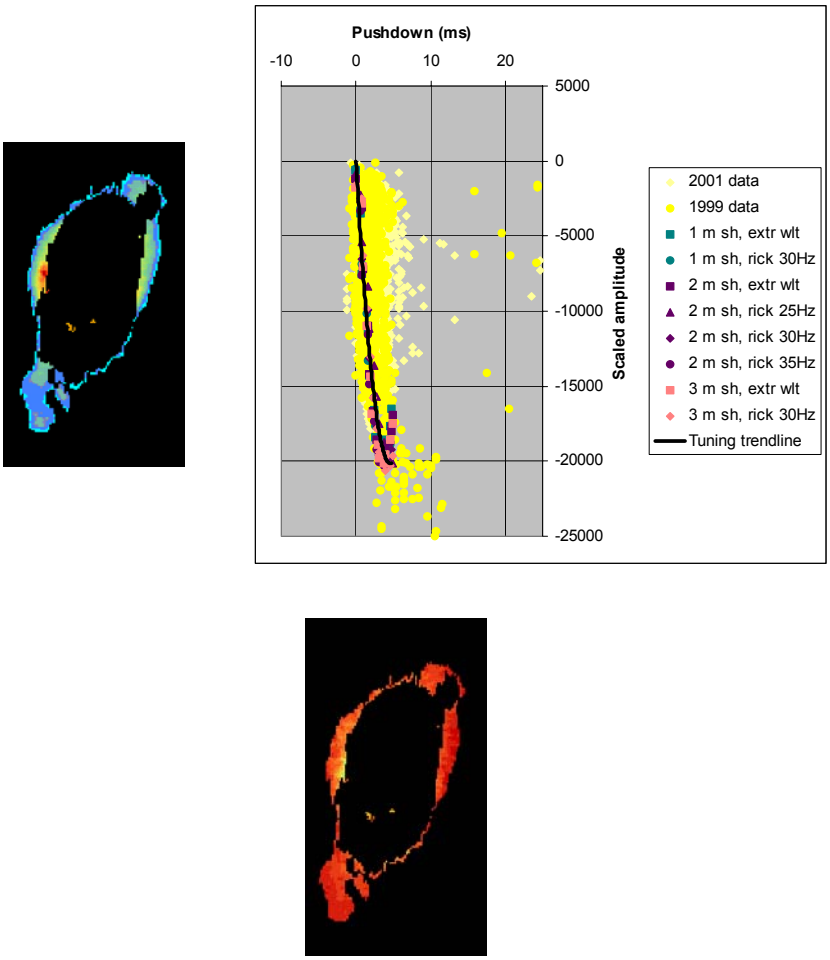

Figure 10: Demonstration of the tuning relationship derived from synthetics and from seismic data (1999 and 2001 survey) originating from locations where only a single CO_2 accumulation is present. The map views show, at these locations, the 1999 seismic amplitudes (left) and the 1999 pushdown (down). The inner black 'shadow' denotes the area of multiple superimposed CO_2 layers.

4.3 CO_2 chimneys

Intriguing detail is visible in parts of the plume (Figure 11). Beneath the gentle closure at the top of the Utsira Sand, the main reflections show the characteristic V-profile velocity pushdown, which builds rapidly downwards. In the southern part of the plume, a vertical column of reduced horizon reflectivity corresponds precisely to a more localised pushdown, itself superimposed on the broader V-profile. The amount of this localised pushdown increases rapidly downwards from the reservoir top to reach a maximum of about 20 ms at about 970 ms two-way time. It does not clearly change beneath this, but tends to smear somewhat, becoming rather diffuse at base Utsira level. The feature is interpreted as a vertical 'chimney' of moderate or high CO_2 saturation, in the upper part of the plume. This causes a rapid build-up of pushdown within the chimney itself and a pushdown shadow below. Similar, though much less prominent seismic features seen elsewhere in the plume are interpreted as smaller CO_2 chimneys.

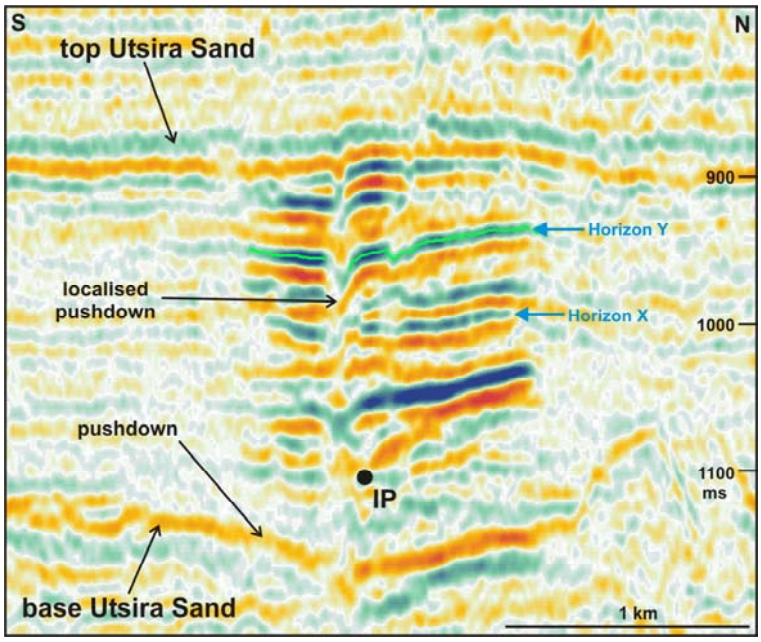

Figure 11: Inline through the 1999 dataset. Note velocity pushdown at base of reservoir and also more localised pushdown interpreted as caused by a "chimney" of CO_2 in the upper part of the plume. Also note lateral amplitude variations on the individual reflectors (e.g. Horizon Y with autopick). IP is the approximate location of the injection point corrected for the pushdown.

The relationship of the main CO_2 chimney to the surrounding reflective layers is exemplified by Horizon 5 (Figure 11). The horizon dips in two-way time towards the chimney, due to the velocity pushdown in the axial parts of the plume. Horizon Y is the most extensive individual reflection within the plume and in plan view shows marked lateral amplitude variations (Figure 12a).

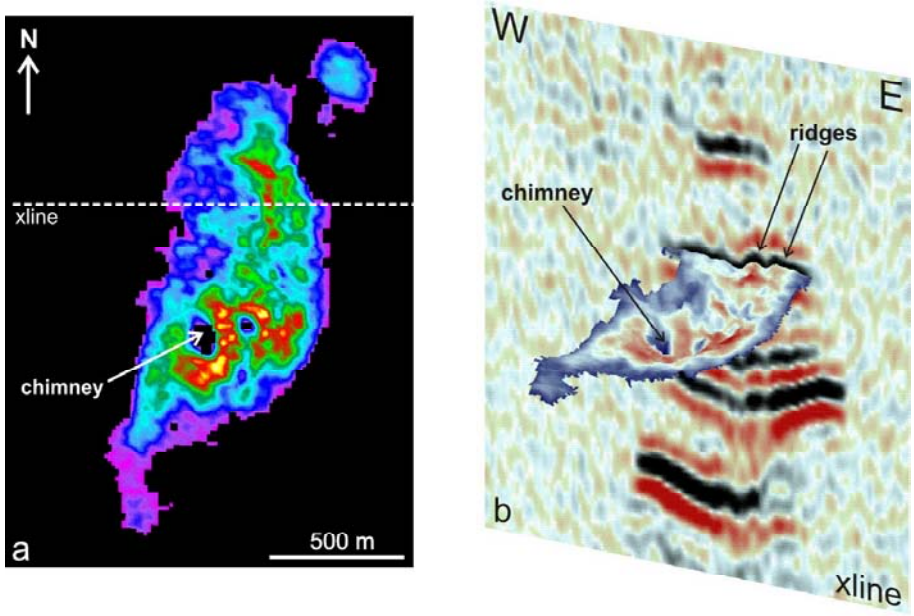

Figure 12: Images of Horizon 5. a) Plan view of reflection amplitude (highest amplitudes in yellow). b) Perspective view from the SSE. Display shows reflection amplitude blue (low) to red (high), draped over two-way time topography. Note the prominent velocity pushdown depression around the chimney, and the high amplitudes corresponding to the ridge-crests farther north.

The chimney is visible as a 'hole' in the amplitude map where the horizon autotracker has not been able to pick the event (Figure 11). It is surrounded by high amplitude reflections, particularly to the east, where a 'stream' of enhanced reflectivity is prominent to the east and north. A perspective view of the horizon (Figure 12b), with reflection amplitudes draped over its two-way time topography, shows the prominent pushdown depression around the chimney, with linear ridgelike features to the north. The ridge crests correspond to markedly enhanced seismic amplitudes that are interpreted as due to small changes in thickness of the CO_2 layer. Thus CO_2 migrating laterally away from the chimney, beneath a thin shale, forms thicker 'ponds' beneath local topographic culminations. These give rise to higher reflection amplitudes as the CO_2 layer approaches the tuning thickness (Figure 13).

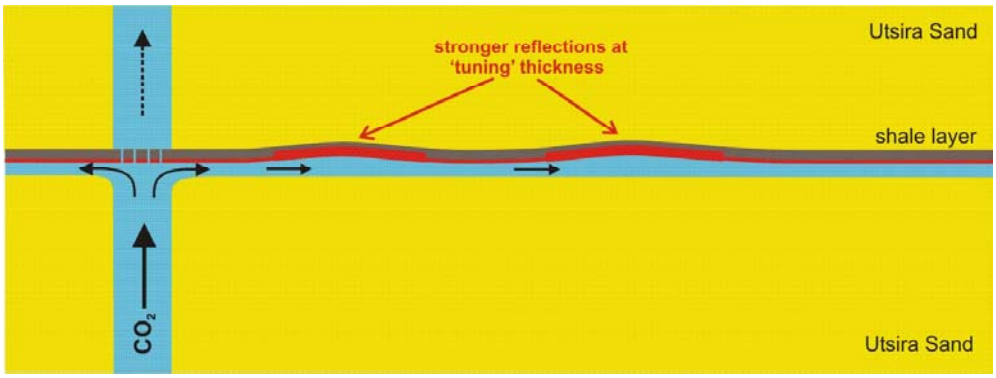

Figure 13: Schematic representation of the vertical CO_2 chimney acting as a feeder to a laterally migrating layer of CO_2 trapped beneath a thin bed of shale. Slight undulations in the shale give rise to ponds of thicker CO_2 and enhanced 'tuning' reflectivity.

Their ridgelike morphologies may be put down to primary sedimentary, channel-related structures within the Utsira Sand, or, perhaps more likely, to differential compaction within what remain largely unconsolidated strata (Zweigel et al. 2001, (in press)). Whatever their underlying cause, it is likely that the amplitude variations are effectively mapping thickness changes in the CO_2 layer down to less than one metre, which more-or-less corresponds to the noise threshold.

It is notable that the main CO_2 chimney is situated nearly, though not perfectly, above the injection point (Figure 11), close to the outer limit of the 95% confidence ellipse of the well position. It is tempting to suppose that the chimney location is linked directly to that of the injection point, however, because of the positional uncertainty, some form of pre-existing geological control cannot be ruled out.

4.4 Determination of the pushdown

The total velocity pushdown observed below the CO_2 for the 1999 survey and for the 2001 survey (Figure 14) gives a good overview of the lateral extent of the CO_2 plume present. These maps have been obtained by cross-correlating the seismic signals below the CO_2 plume of the time-lapse surveys with those of the baseline survey.

The shape of the total "push-down" map is similar to the cumulative amplitude contours of the interpreted CO_2 accumulations (Figure 14). This increases our confidence that

amplitude and layer thickness are related by the tuning effect and that even very thin CO_2 layers of the order of 1 metre thick can be detected.

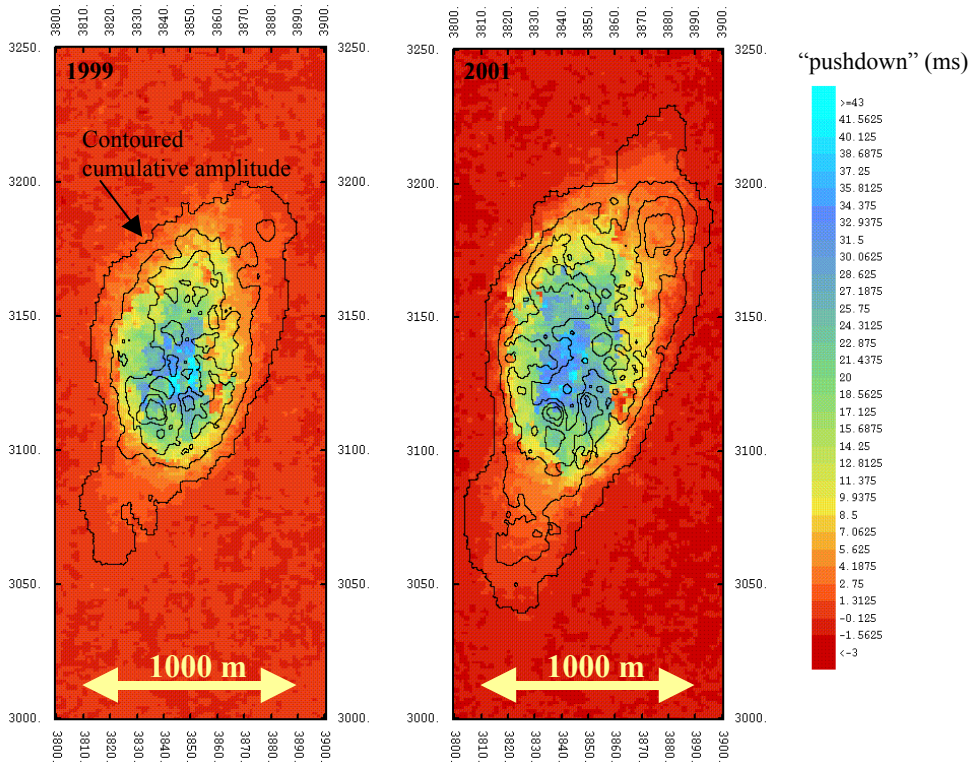

Figure 14: Velocity "push-down" in time (ms), observed below the CO_2 plume in 1999 and in 2001. The "push-down" has been determined by cross-correlating the seismic signals below the CO_2 of respectively the 1999 and the 2001 surveys with the 1994 survey. The isolines indicate the shape of the cumulative (total) seismic amplitude anomaly caused by the injected CO_2.

4.5 Observed differences at 1999 and 2001

The ways in which the CO_2 plume has changed between 1999 and 2001 are quite interesting, in that major growth of the CO_2 accumulations is restricted to the upper part of the plume. Thus, small accumulations in 1999 at top Utsira Sand and level 8 had grown considerably by 2001. Also the largest accumulation in the upper part of the reservoir (level 5) has grown. In contrast, the deeper accumulations (levels 1 and 2) have not changed very much and appear to be in a state approaching equilibrium. One explanation of this is that the major CO_2 chimney is now effectively by-passing the deeper accumulations, with the implication that as a conduit it is becoming more effective with time.

5 Verification aspects

The 4D data provide two essentially independent means of quantitatively assessing the amount of CO_2 in the subsurface. Some aspects of the detailed quantitative interpretation of the 1999 dataset are presented below.

5.1 Thin layer summation

The capillary pressure, P_c, between the formation brine and the injected CO_2 will cause the CO_2 saturation, Sco_2, to vary with height, h, in each CO_2 layer. The gradient can be computed by balancing the buoyancy, $\Delta\rho \cdot g\, h$, with the capillary pressure.

In SI units:

$$\Delta\rho \cdot g \cdot h = P_c = 810.35\,(1 - Sco_2)^{-0.948}$$

The capillary pressure - saturation relationship was determined by centrifuge experiments on core material from the Utsira Sand (SACS unpublished data). The variation of Sco_2 with h was thereby computed and also the average value of Sco_2 for a range of layer thicknesses (Figure 15).

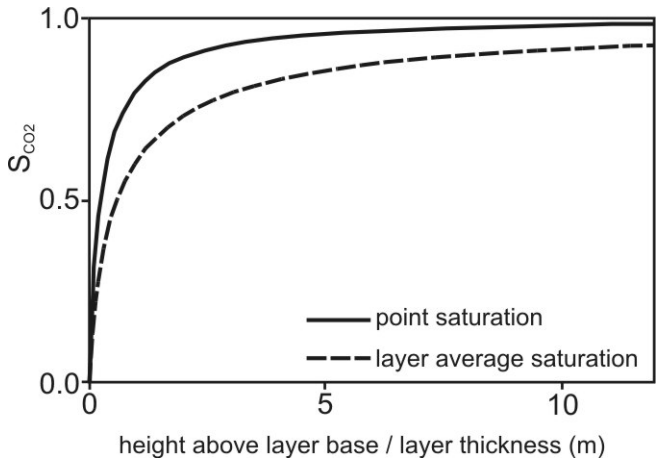

Figure 15: Variation of average CO_2 saturation with layer thickness.

Using this information the layer thicknesses derived for each reflecting horizon can be converted to net CO_2 thickness (e.g. Figure 16).
This was carried out at each grid point (CMP), by multiplying the layer thickness by the average CO_2 saturation (Figure 15), and by the reservoir porosity. Summation of these net thicknesses for each layer gives a first order estimate of the total amount of CO_2 imaged by the seismic data. For the interpretation of the 1999 dataset, the total volume in thin layers is estimated at about 2.6×10^6 m^3; somewhat less than the known injected volume. For the 2001 dataset this volume is estimated at about 4.7×10^6 m^3. A number of factors will contribute to uncertainty in this figure. These include uncertainty in the horizon interpretation (including interference between adjacent tuning wavelets), errors in the simple amplitude to thickness conversion, the presence of dispersed (essentially unreflective) CO_2 in between the reflective layers, dissolution of CO_2 into the formation

water and amplitude loss in the deeper plume due to signal attenuation; or by a combination of these factors.

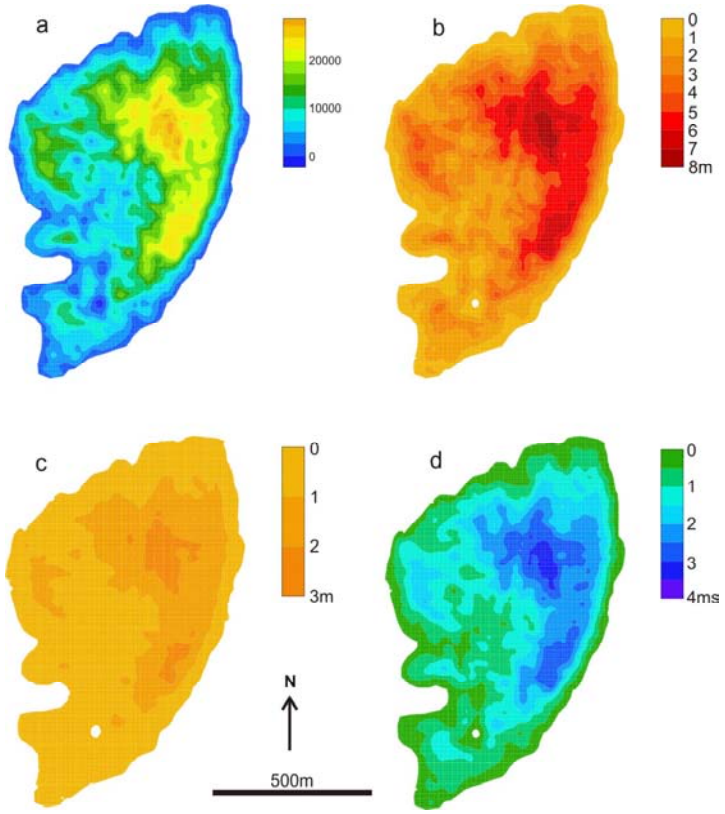

Figure 16: Plan views of CO_2 accumulation 1 (Horizon X). a) reflection amplitude b) thickness of rock - CO_2 layer c) net thickness of CO_2, assuming $\Phi = 0.37$ and saturation-thickness function d) velocity pushdown (ms) due to layer.

5.2 Velocity Pushdown

The velocity pushdown of reflections beneath the CO_2 plume (Figure 17) provides an alternative means of estimating CO_2 volume in situ. By interpreting the base Utsira Sand beneath the plume on both the 1994 and time lapse surveys it is possible to map the pushdown beneath much of the CO_2 plume (Figure 17c). Significant uncertainty arises however because reflections on the time lapse data are locally degraded and the mapping shows some instability beneath the outer parts of the plume where pushdown values are small. An alternative approach is to map the pushdown automatically by cross-correlating a window of the sub-plume reflections on the 1994 and time lapse surveys, and thereby deriving a pushdown time-lag for each seismic trace (Fig 17d). Pushdown values derived in this way are more stable than the interpreted map beneath the outer parts of the bubble, but high pushdown values directly beneath the main CO_2 chimney are not resolved, due to degradation of the cross-correlogram by poor signal to noise ratios. Irrespective of the method of derivation, the pushdown anomaly is elliptical in plan both for the 1999 and the 2001 datasets, with time-lags in excess of 20 ms widely observed beneath the central parts of the plume and locally in excess of 40 ms. The total amount of pushdown caused by the plume can be expressed as the individual time-lags at each CMP trace (or bin), summed over the entire anomaly. This

is termed the Total Area Integrated Time Delay (TAITD). The pushdown mapped for the 1999 dataset by interpretation of the Base Utsira Sand (Figure 17c), has a TAITD of about 11000 m^2s, whereas the pushdown mapped by cross-correlation (Figure 17d) has a TAITD value of about 9200 m^2s. Optimal mapping of the pushdown would probably incorporate both cross-correlation and local manual picking with a likely intermediate value of TAITD.

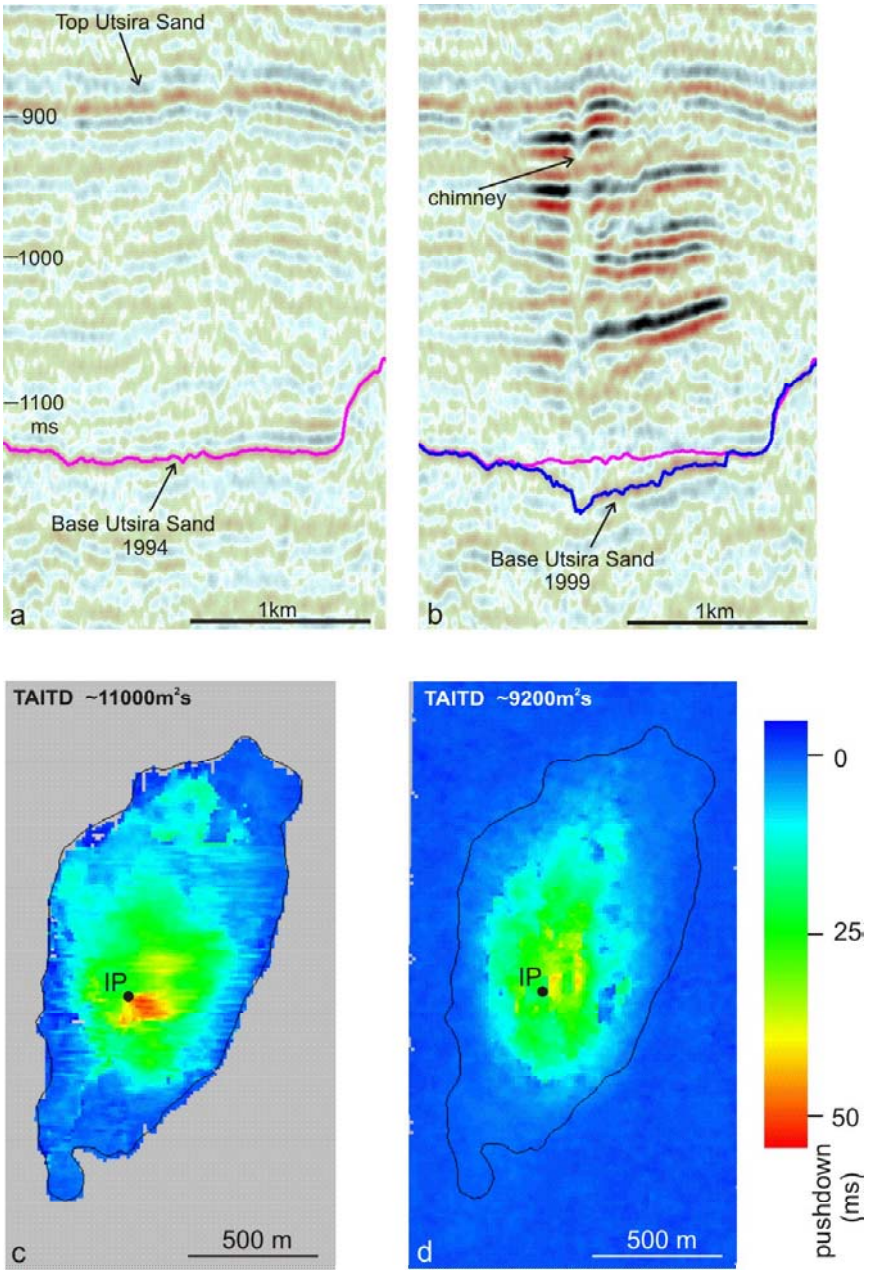

Figure 17: Velocity pushdown beneath the CO_2 plume. a) 1994 inline showing base Utsira Sand pick. b) 1999 inline showing base Utsira Sand pick (1994 pick for reference). Note higher pushdown beneath chimney. c) Map of two-way time pushdown based on manual interpretation of Base Utsira Sand (note high pushdown values SE of the injection point, beneath the main chimney) d) Map of pushdown based on cross-correlation of a window of events beneath the plume (note lack of high pushdowns associated with the chimney). IP denotes injection point. Black outline denotes interpreted 'footprint' of plume envelope.

The amount of pushdown can be related algebraically to the column of CO_2 in the overlying strata (Figure 18).

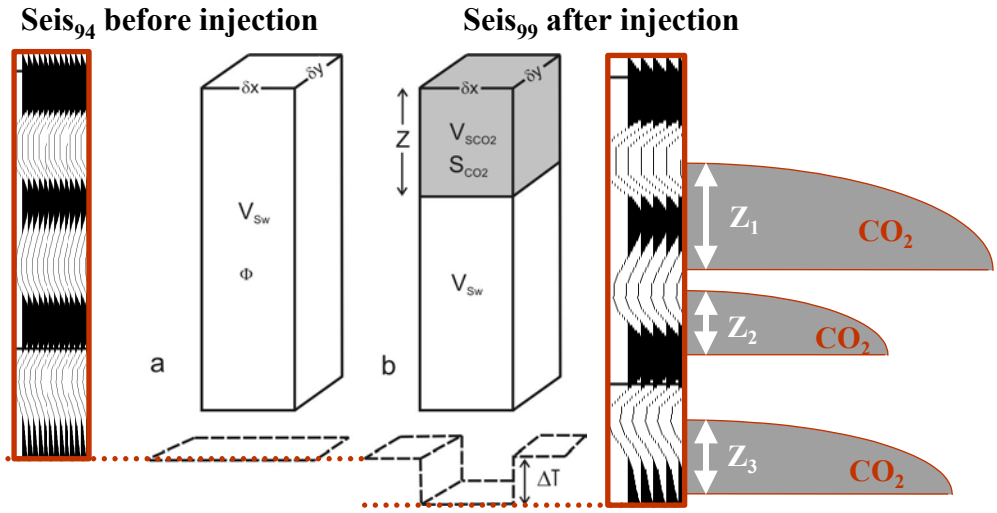

Figure 18: Schematic views of a vertical column of rock corresponding to a single cmp bin, underlain by a notional flat reflector (dashed, shown in two-way time). a) Rock column saturated with water. b) Partial replacement of water by CO_2 produces velocity pushdown ΔT

For each grid point (CMP):

$$\Delta T \cdot \delta x \cdot \delta y = \frac{2\left(V_{SW} - V_{SCO2}\right) \cdot Z \cdot \delta x \cdot \delta y}{\left(V_{SW} \cdot V_{SCO2}\right)}$$

where:

ΔT is the time delay at each trace (T^{99}survey – T^{94} survey)
δx = x-dimension of bin (12.5 m for the SACS data)
δy = y-dimension of bin (12.5 m for the SACS data)
Vsw = seismic velocity of water-saturated rock
V_{SCO2} = seismic velocity of rock saturated with CO_2 (at saturation Sco_2)
Z = thickness of rock saturated with CO_2 (at saturation Sco_2)

Substituting reservoir porosity (ϕ) and CO_2 saturation (Sco_2) and summing all the grid points over the whole pushdown anomaly:

$$\sum \Delta T \cdot \delta x \cdot \delta y = \frac{2\left(V_{SW} - V_{SCO2}\right) \cdot \left(Total\ injected\ volume\ of\ CO_2\right)}{\left(V_{SW} \cdot V_{SCO2}\right) \cdot \phi \cdot S_{CO2}}$$

In principal therefore, the Total Area Integrated Time Delay ΣΔT·δx·δy, as measured from the seismic data (Figure 17c,d) can be related directly to the total volume of CO_2 in the plume. In practice however there are significant uncertainties, particularly with respect to the expression below, here termed the 'Pushdown Factor':

$$\frac{2\left(V_{SW} - V_{SCO2}\right)}{\left(V_{SW} \cdot V_{SCO2}\right) \cdot \phi \cdot S_{CO2}}$$

The Pushdown Factor has units of sm^{-1} and expresses the amount of pushdown in seconds (or, more conveniently, milliseconds), per net metre thickness of CO_2. [N.B. cf. the Gross Pushdown Factor defined earlier which expresses the amount of pushdown in seconds (or milliseconds) per metre thickness of CO_2 saturated rock].

To calculate the Pushdown Factor, seismic velocities in rock filled with CO_2 at various saturations have been estimated using the Gassmann fluid substitution equations assuming a value for K_{CO2} of 0.0675 GPa (Figure 6). Errors are related mostly to uncertainties in elastic parameters, principally the bulk moduli of the rock framework and of supercritical CO_2. Pressure effects on the seismic velocities are expected to be negligible. No significant increase in pressure has been observed during the injection process so far, the CO_2 flowing easily into the very high permeability reservoir. The pressure-temperature conditions of the reservoir around the CO_2 plume are such that the CO_2 is expected to remain in a supercritical state.

Direct observation of velocity pushdown within the plume lends support to the Gassmann analysis. Around and within the CO_2 chimney in the upper part of the plume (Figure 12), a total pushdown of 22 ms develops over an estimated 60 m section of reservoir sand. This requires a seismic velocity of about 1450 ms^{-1} within the chimney, broadly consistent with Gassmann-derived values for CO_2 saturations in the range 0.3 to 1.0 (Figure 6). This is in line with both the moderate saturations for vertical conduits proposed by Johnson et al. (2001) and the higher saturations indicated by Lindeberg et al. (2001). Overall, sensitivity analysis suggests that velocity error does not comprise the main source of uncertainty in calculating the Pushdown Factor (see below).

Most of the velocity decrease induced by CO_2 takes place at low saturations, the velocity curve levelling out at values of Sco_2 greater than about 0.3 (Figure 6). This inherent ambiguity, together with the fact that Sco_2 is an explicit term in the Pushdown Factor, renders the value of Sco_2 the main source of uncertainty in the pushdown calculation. The Pushdown Factor varies from over 25 milliseconds per net metre of CO_2 at very low saturations of CO_2, to only 1 – 2 milliseconds per net metre of CO_2 at high saturations. For a fixed total amount of CO_2 low saturations are therefore a much more efficient pushdown agent than higher CO_2 saturations. This leads to inherent uncertainty; to calculate the pushdown from a known injected volume, it is necessary also to know the effective saturation of CO_2 throughout the plume.

Forward modelling can be used to address the problem. TAITDs have been calculated for a series of assumed plume saturation scenarios based on the total volume of the plume envelope in 1999 (Figure 19). The two saturation 'end-members' will be considered first. The minimum saturation case is represented by CO_2 distributed homogeneously throughout the entire volume of the plume envelope (Figure 19a). The CO_2 has a uniformly low saturation ($Sco_2 = 0.075$) and generates a TAITD of 30802 m^2s. This represents the theoretical maximum possible pushdown for the injected volume of CO_2 and the observed plume geometry. The opposite end-member is the maximum saturation case, where CO_2 is present only in a state of full saturation ($Sco_2 = 1.0$), such as in discrete fully saturated layers (Figure 19b). The TAITD in this case is only 3801 m^2s, which represents the minimum theoretical pushdown for the known

injected volume of CO_2. Neither of the end-member scenarios matches the observed TAITD values. The low saturation end-member generates a pushdown that is much too high, and moreover, is not realistic in terms of the observed plume reflectivity. The full saturation end-member produces a pushdown that is much too low.

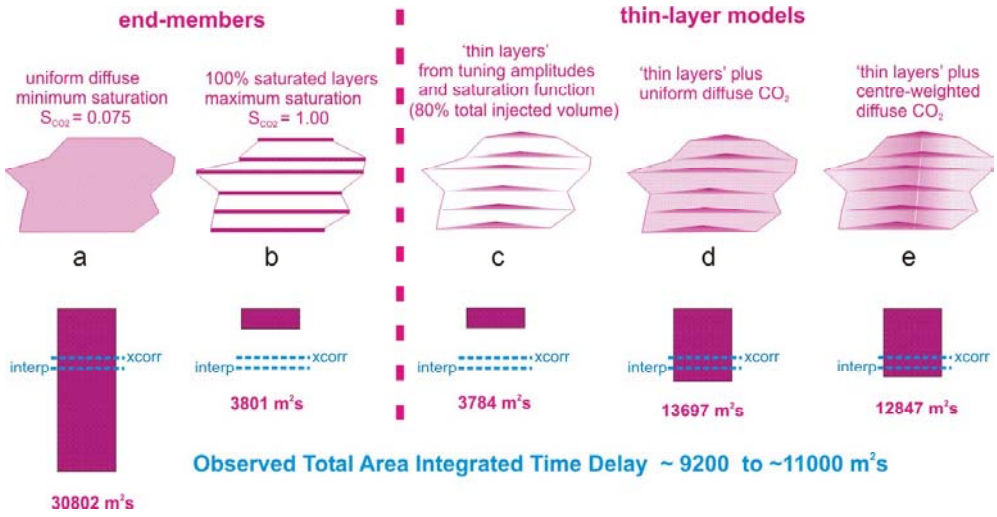

Figure 19: Computed total area integrated time delays for 3.3 x 10^6 m^3 of injected CO_2 in different plume saturation models. a) CO_2 distributed homogeneously throughout the plume volume b) CO_2 present only in fully saturated form e.g. in layers c) CO_2 as given by thin layer summation and saturation function (i.e. ~80% of the injected volume) d) CO_2 as in (c), but with remaining CO_2 dispersed uniformly between layers e) CO_2 as in (c) but with remaining CO_2 dispersed between layers and concentrated preferentially in axial part of plume. Observed TAITD as blue dashed lines (interp from interpreted Base Utsira Sand, xcorr from cross-correlation).

Because the observed TAITD does lie between the end-member saturation limits, it can, therefore, be modelled by some intermediate saturation distribution. Bearing in mind the observed reflectivity, a reasonable saturation scenario is one whereby CO_2 in the plume is partitioned into two separate components: a 'reflective' component of CO_2 trapped in thin layers, each obeying the thickness-saturation function (Figure 15), and an 'unreflective' component of diffuse, low saturation CO_2, which occupies all or part of the volume in between the layers.

Models based on this scenario took the component of CO_2 in layers as the volume calculated by thin layer summation (see above). From this, the time-lag was calculated, using the layer thickness-saturation function, at each CMP, for each horizon (e.g. Figure 6d). The TAITD for the component of CO_2 in layers was then obtained by summing over all horizons, giving a value of 3784 m^2s (Figure 19c). This is much lower than the observed TAITDs, but the model is incomplete, in that it contains only about 80% of the total injected amount of CO_2. Additional pushdown will result from the remaining 20% of CO_2, which is assumed to present as a diffuse, low-saturation component, in between the layers.

The simplest two-component model (Figure 19d) assumes that the remaining diffuse CO_2 is homogeneously distributed throughout the intra-layer volume. The additional pushdown due to this diffuse CO_2 is 9913 m^2s, amply demonstrating the very high pushdown efficiency of low saturation CO_2. The resultant TAITD of 13697 m^2s is however considerably higher than the observed range of 9200 - 11000 m^2s. A

refinement of the model can be effected by the intuitively reasonable step of preferentially concentrating the diffuse CO_2 in the central, axial parts of the plume. A simple concentric saturation distribution, increasing linearly from $Sco_2 = 0.0$ at the plume edge, to $Sco_2 \sim 0.06$ at the plume centre (Figure 19e) gives the same total injected volume but with a TAITD of 12847 m^2s, significantly closer to the observed range. Further increasing the heterogeneity of the diffuse CO_2 component, by concentrating it into localised volumes of higher saturation, has the effect of decreasing the overall pushdown. Thus, the likely presence of chimneys of CO_2 would effect a further reduction in the calculated pushdown, possibly to the observed values. Alternatively, an observed pushdown lower than the calculated value may simply signify that rather more CO_2 is trapped in the thin layers, at high saturations, than is indicated by the simple amplitude-thickness transformation. The effects of dissolution should not be discounted either, because dissolved CO_2 would effectively become seismically invisible, rendering observed pushdowns smaller than predicted. Johnson et al. (2001) indicate however that in the first three years of injection, even with lateral dispersal of CO_2 by trapping beneath shales, amounts of CO_2 dissolving in the formation waters are likely to be small (<5%).

5.3 Pushdown - Amplitude relationships

In the above, reflection amplitudes and velocity pushdown give estimates of in situ CO_2 volume that are essentially independent. It is also fruitful to examine these two seismic parameters together, as their inter-relationships provide additional useful insights.

Velocity pushdown increases strongly towards the centre of the plume with a pronounced area of elevated values (>40ms) around and east of the injection point (Figure 20a). Total plume amplitudes show a different pattern however (Figure 20b), particularly across the central part of the plume where they are more evenly distributed, without notably increased values east of the injection point. This different behaviour can be quantified as variation in the pushdown – amplitude ratio (Figure 20c).

The pushdown - amplitude ratio is analogous to the Pushdown Factor in that it measures pushdown per unit total reflection amplitude, where the latter is related to total CO_2 layer thickness. The observed variation of pushdown – amplitude ratio (Figure 20c) can therefore be interpreted as providing qualitative insights into saturation distribution. The outer parts of the plume, particularly in the NE and SW, farthest from the injection point, are characterised by low pushdown – amplitude ratios. These are interpreted as areas where CO_2 is present only at high saturations in thin, reflective layers, which produce relatively small amounts of pushdown (cf Figure 18). In contrast, the inner parts of the plume show much higher ratios. These are interpreted as signifying the presence of diffuse, low saturation CO_2 between the layers, producing additional pushdown but no additional reflectivity.

A further effect, which would tend to reinforce the observed pattern, is a possible reduction in layer reflectivity where diffuse CO_2 decreases the acoustic contrast of the high saturation layers. This is exemplified by the main CO_2 chimney, which with its high pushdown, but subdued reflectivity (Figure 16), is marked by a prominent localised area of high pushdown – amplitude ratio (Figure 20c).

The various effects therefore are quite complex, but the underlying pattern is clear; elevated pushdowns in the central part of the plume do not correspond to similarly enhanced reflectivity, and thereby indicate the presence of diffuse, unreflective CO_2. This very much supports the preferred saturation model of Figure 19e.

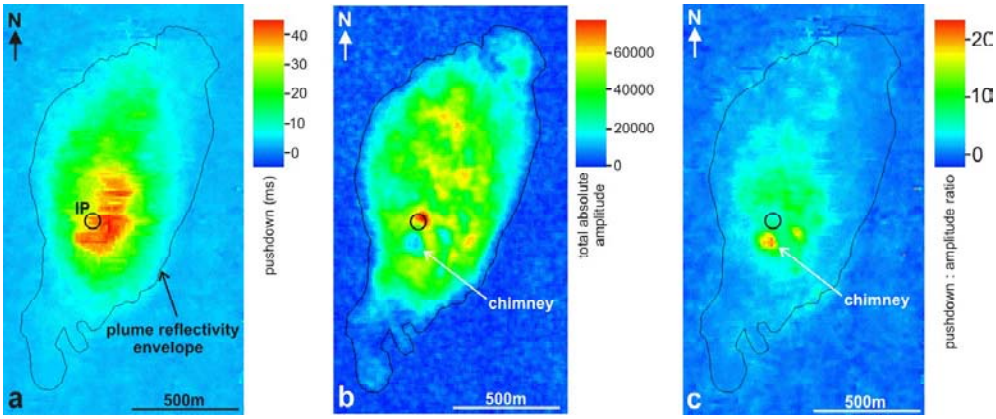

Figure 20: a) Two-way time pushdown beneath the plume (IP denotes injection point). Mapping incorporates both cross-correlation and manual interpretation b) Total absolute reflection amplitude of the plume from seismic difference data (analysis window 850 –1070ms) c) Pushdown - amplitude ratio i.e. [grid(a) / grid (b)]. Black outline denotes outer edge of the plume reflectivity envelope.

The relationship therefore velocity pushdown and plume reflectivity is a potentially useful tool for mapping saturation distributions within the plume.

6 From reservoir simulation to synthetic seismics

6.1 Reservoir simulation model

Based on the seismic interpretation a full-field 3D reservoir simulation model has been constructed (van der Meer et al., 2001). This was not a straightforward task, taking into account that the intra reservoir shale layers could only be interpreted on the time-lapse surveys with CO_2 present below them. Moreover these interpretations were in two-way traveltime and had to be time-depth converted for the simulation model. With the large velocity variations occurring in the reservoir due to the presence of CO_2 an accurate time-depth conversion was not feasible and an accurate depth model of each individual shale layer could not be obtained. To circumvent this problem these intra shale layers have been assumed parallel to the upper shale layer just below the top of the reservoir.
The total simulation model covers an area of 15.7 km^2. The Utsira Sand was represented by a total of 59 layers. The shale layers were represented in the model by transmissibility modifiers between the appropriate layers. The result of the simulation after three years of injection, at the time of the first time-lapse seismic survey in October 1999, has been shown in Figure 3.

6.2 Synthetic seismics derived from the reservoir simulation model

The resulting saturation model was transformed into a 3D acoustic impedance model using the Gassmann relations in order to perform a forward seismic modelling. The process has been schematised in Figure 21.

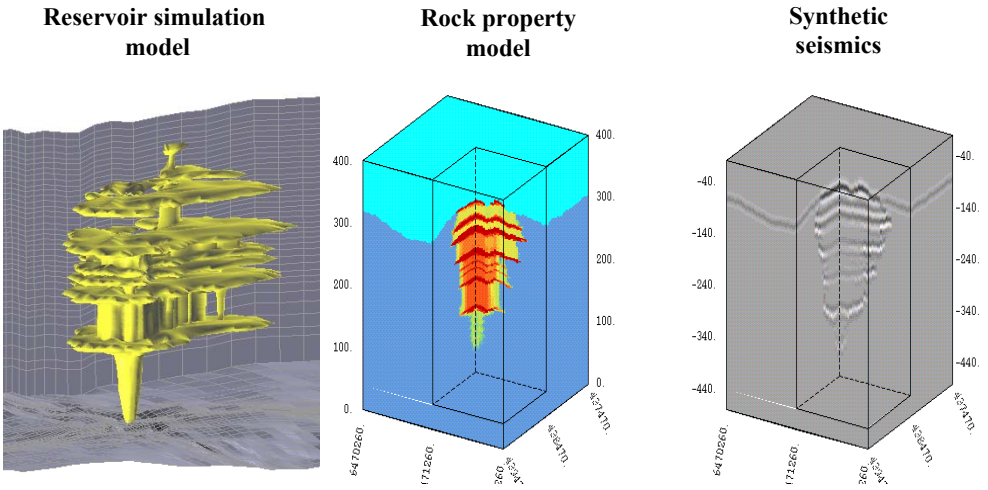

Figure 21: Scheme of the adopted workflow. The 1999 reservoir simulation model (left) containing saturations is transformed into an acoustic rock property model using Gassmann (middle). The acoustic model has been used for synthetic seismic modelling (right).

A cross-section for the 2001 model, representing crossline 3123, is shown in Figure 22. The leftmost image represents the acoustic impedance model in depth, the middle image

is the synthetic seismic data and the rightmost image corresponds to the seismic field data both in two-way traveltime.

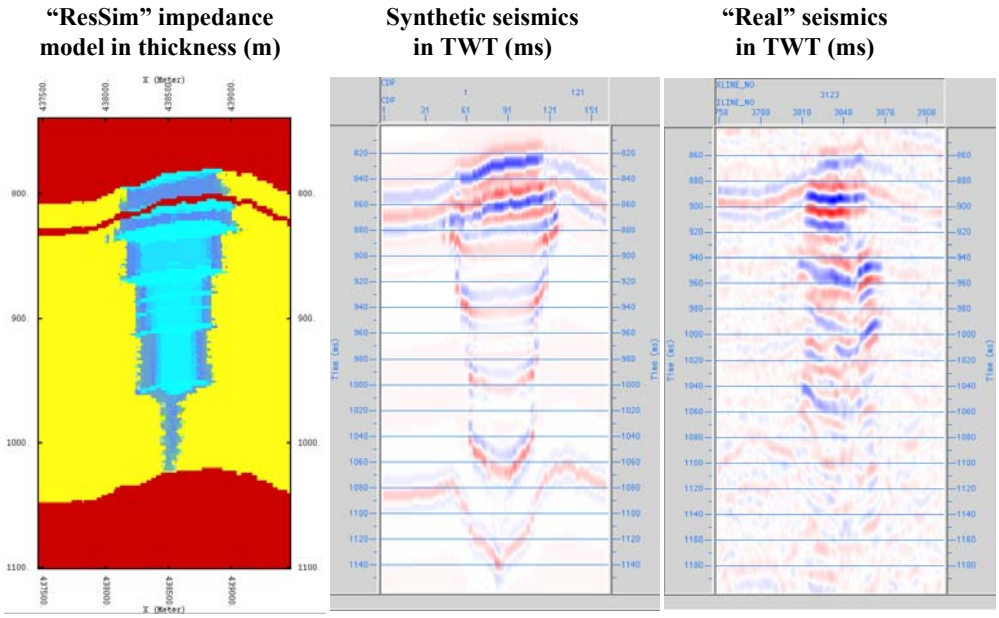

Figure 22: Cross section from west to east of the 2001 acoustic impedance model derived from the 2001 reservoir simulation model in depth (left), the synthetic seismic data (middle) and the corresponding 2001 seismic data both in two-way traveltime.

Taking into account the assumptions made to construct the model, the synthetic seismic data mimic the field data fairly well. The pushdown effect is clearly demonstrated on the synthetic seismic data. Figure 23 shows the lateral extent of the pushdown anomalies respectively for the 1999 seismic data, for the 2001 seismic data and for the synthetic data.

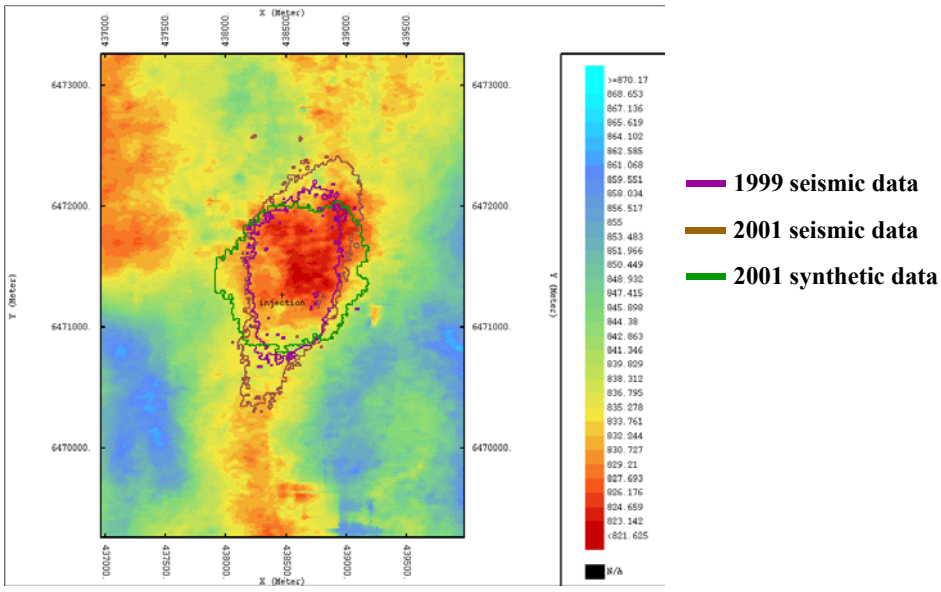

Figure 23: Topography of the five metre shale layer (level 8) with the outlines of the pushdown anomalies as observed in the 1999 dataset (purple), in the 2001 dataset (brown) and in the2001 synthetic seismic data (green) superposed.

The observed-data show a more north-south elongated shape, whereas the synthetic data follow the domal shape of the upper shale layer (level 8) topography. This effect can also be observed on the synthetic data shown in Figure 22. The lateral extent of the CO_2 anomaly on the east-west synthetic data of crossline 3123 is larger than on the observed data.

6.3 Analysis of the results

The resulting synthetic seismic data can be compared to the observed seismic data. Differences can be used to optimise the reservoir simulation model. Through an iterative refinement an optimal model and/or interpretation could theoretically be obtained. In practice the optimisation loop is not straightforward due to the uncertainties both in the topography of the shale layers and on the seismic velocities.

As already stated, the synthetic seismic data match the observed data fairly well. The resulting pushdown derived from the synthetic data can be compared to the observed seismic data as well. This is done for the 2001 dataset in Figure 24.

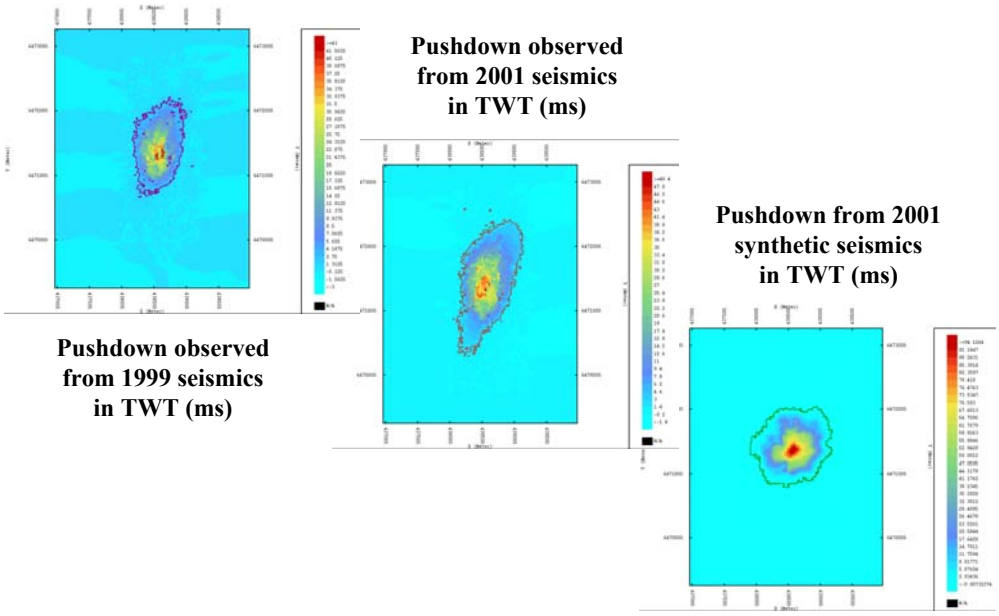

Figure 24: Pushdown observed in the 1999 time lapse seismic data (left), in the 2001 seismic data and in the synthetic data derived from the 2001 reservoir simulation model. When comparing the latter two the pushdown observed in the synthetic data appears to be too large with respect to the field data.

Note that the pushdown derived from the 2001 reservoir simulation model is larger than the one observed in the field data. This is mainly caused by the relatively high concentrations (up to 10%) of CO_2 in between the shale layers over large areas. In principle four different aspects (can) play a role (in order of likelihood):

- The velocity of the CO_2 saturated rock is not correct. Note that the distribution of the CO_2 can influence the "mean velocity" of the P-waves through the reservoir. More patchy saturation distributions (compared to the seismic wavelength) will generally lead to higher velocities and thus to less pushdown. This factor is very likely to influence the results.

- The area or lateral extent over which the CO_2 is distributed in the reservoir simulation model is too small with respect to the observed extent. With the same total amount of CO_2 injected in both cases this leads to more CO_2 per seismic bin in the synthetic case and thus too much pushdown. This is caused by the assumption on the topography of the intra shale layers.
- In reality part of the CO_2 is dissolved in water. Recent reservoir simulations, taking solubility during simulation into account, indicated up to 5% of the total amount of CO_2 in solution in 2001 (personal communication Bert van der Meer). This implies too much CO_2 in the simulation model and thus too much pushdown.
- The relative permeabilities in the reservoir simulation are not correct leading to too high concentrations of CO_2. This is not very likely since sensitivity analysis indicates a minor influence of the relative permeability curves on the saturations.

7 Discussion and conclusions

The most important conclusion to be taken from the seismic monitoring at the Sleipner underground CO_2 storage site is probably that time-lapse seismic data enables us to map the CO_2 distribution clearly and to image pathways in time. The effective detection limit for local CO_2 accumulations is of the order of a metre or less. Such resolution makes us confident that any significant leakage into the Pliocene shales would have been picked up by the data.

The velocity pushdown effect provides a powerful means of estimating the volume of CO_2 in situ, albeit with uncertainties related to non-uniqueness. The tuning phenomenon enables effective thin-bed resolutions down to about a metre and provides a quantitative tool for volumetric estimation independent of the pushdown analysis.

The interpreted seismic data has been used for a full 3D reservoir simulation model. The construction of such a model was very difficult for two main reasons:

- The intra-reservoir shale layers could only be interpreted on the repeat time-lapse surveys with CO_2 present.
- The conversion from time to depth of these intra-reservoir shale layers is not sufficiently accurate due to the large velocity variations caused by the presence of CO_2.

As a consequence, it was necessary to estimate the topography of the intra-reservoir shale layers by supposing them parallel to the five metre shale layer, the only one that has been interpreted on the baseline seismic data. For the longer-term predictions (>10 years) the reservoir simulation model is more reliable. As is already observed for the lower intra-reservoir shale layers, a kind of steady-state flow towards the top of the reservoir may eventually be established. Then the main lateral migration of CO_2 will be governed by the topography of the top Utsira Sand, which has been mapped accurately.

From the seismic data analysis and the results of the reservoir simulation the following conclusions can be drawn:

- Based on the currently used Gassmann parameters a percentage in the order of 10 to 20% of diffuse (low-saturation) CO_2 in between the intra-reservoir shale layers is required to produce the observed amount of pushdown.
- The saturation of the diffuse CO_2 increases towards the middle of the plume (from zero at the plume edges) as indicated by Figures 19 and 20.
- The current simulation model shows similar characteristics, but saturations differ in detail.

Part of the next phase of work within the CO2STORE project is to examine the reservoir simulations in detail with respect to the distribution of diffuse CO_2 and how this relates to the location of the main chimney (and minor chimneys too). Updating of both the seismic data interpretation, the reservoir simulation models and the rock physics (Gassmann) relations will be carried out with the gathering of new data (such as the 2002 seismic data and the gravity data).

8 References

Arts, R.J., 2000. Note on the seismic data. Internal SACS report, reference number NITG 00-237-B.

Arts, R., Brevik, I., Eiken, O., Sollie, R., Causse, E., & van der Meer, L. 2001: Geophysical methods for monitoring marine aquifer CO_2 storage - Sleipner experiences. In: D.J. Williams, R.A. Durie, P. McMullan, C.A.J. Paulson & A.Y. Smith (eds): Greenhouse Gas Control Technologies, CSIRO Publishing, Collingwood, Australia, 366 – 371.

Arts, R, Eiken, O., Chadwick, A., Zweigel, P., van der Meer, L., Kirby, G., (in press). Seismic monitoring at the Sleipner underground CO_2 storage site (North Sea). In: S.J. Baines & R.H. Worden (Eds): Geological storage of CO_2 for emissions reduction. Geological Society, London, Special Publication.

Arts, R., Elsayed, R., van der Meer, L., Eiken, O., Ostmo, S., Chadwick, A., Kirby, G., Zweigel, P., Zinszner, B., 2002: Estimation of the mass of injected CO_2 at Sleipner using time-lapse seismic data.. 64th EAGE meeting, Florence, paper H016.

Arts, R. J., Zweigel, P., & Lothe, A.E. 2000: Reservoir geology of the Utsira Sand in the Southern Viking Graben area – a site for potential CO_2 storage.- 62nd EAGE meeting, Glasgow, paper B-20.

Brevik, I., Eiken, O., Arts, R.J., Lindeberg, E., & Causse E. 2000: Expectations and results from seismic monitoring of CO_2 injection into a marine acquifer. 62nd EAGE meeting, Glasgow, paper B-21.

Chadwick, R.A., Holloway, S., Kirby, G.A., Gregersen, U. & Johannessen, P.N. 2001. The Utsira Sand, Central North Sea – an assessment of its potential for regional CO_2 disposal. In: D.J. Williams, R.A. Durie, P. McMullan, C.A.J. Paulson & A.Y. Smith (eds): Greenhouse Gas Control Technologies, CSIRO Publishing, Collingwood, Australia, 349 – 354.

Chadwick, R.A., Arts, R., Eiken, O, Kirby, G.A., Lindeberg, E. & Zweigel, P. (in press). 4D seismic imaging of an injected CO_2 plume at the Seipner Field, central North Sea. In: Davies, R., Cartwright, J., Stewart, S., Underhill, J and Lappin, M. (eds.) 3D Seismic Data: Application to the Exploration of Sedimentary Basins. Memoir of the Geological Society, London.

Eiken, O., Brevik, I., Arts. R., Lindeberg, E., & Fagervik, K., 2000: Seismic monitoring of CO_2 injected into a marine aquifer. SEG Calgary 2000 International conference and 70th Annual meeting, Calgary, paper RC-8.2.

Gassmann, F., 1951. Uber die Elastizitat poroser Medien. Vier, der Natur, Gesellschaft in Zurich, 96, 1-23.

Gregersen, U.; Michelsen, O. & Sørensen, J.C. 1997: Stratigraphy and facies distribution of the Utsira Formation and the Pliocene sequences in the northern North Sea. Marine and Petroleum Geology, 14, 893-914.

Johnson, J.W., Nitao, J.J., Steefel, C.I., and Knauss, K.G., 2001, Reactive transport modeling of geologic CO2 sequestration in saline aquifers: the influence of intra-aquifer shales and the relative effectiveness of structural, solubility, and mineral trapping during prograde and retrograde sequestration: Proceedings of the First National Conference on Carbon Sequestration, Washington, DC, May 14-17, 2001, 60 p., UCRL-JC-146932.

Lindeberg, E., Zweigel, P., Bergmo, P., Ghaderi, A., & Lothe, A., 2001. Prediction of CO_2 dispersal pattern improved by geology and reservoir simulation and verified by time lapse seismic. In: D.J. Williams et al. (eds.): Greenhouse Gas Control Technologies, CSIRO Publishing, Collingwood, Australia, pp. 372-377.

van der Meer, L.G.H., Arts, R.J., Peterson, L., 2001. Prediction of migration of CO_2 injected into a saline aquifer: Reservoir history matching to a 4D seismic image with a compositional Gas/Water model. In: D.J. Williams, R.A. Durie, P. McMullan, C.A.J. Paulson & A.Y. Smith (eds): Greenhouse Gas Control Technologies, CSIRO Publishing, Collingwood, Australia, 378-384.

Zweigel, P., Arts, R., Bidstrup, T., Chadwick, A., Eiken, O., Gregersen, U., Hamborg, M., Johanessen, P., Kirby, G., Kristensen, L., & Lindeberg, E., 2001: Results and experiences from the first Industrial-scale underground CO2 sequestration case (Sleipner Field, North Sea). American Association of Petroleum Geologists, Annual Meeting, June 2001, Denver, abstract volume (CD) 6p.

Zweigel, P., Arts, R, Lothe & A.E. Lindeberg, E., (in press). Reservoir geology of the Utsira Formation at the first industrial-scale underground CO_2 storage site (Sleipner area, North Sea). In: S.J. Baines & R.H. Worden (Eds): Geological storage of CO_2 for emissions reduction. Geological Society, London, Special Publication.